

# **Shot-to-Shot Backscatter Monitor for Intensity-Position Measurement at the European XFEL**

Pavel Volkov, Moscow Institute of Physics and Technology, Russia  
Supervisors: Jan Gruenert, Cigdem Ozkan, European XFEL GmbH

September 8, 2011

## **Abstract**

Possibilities for Compton-scattering based non-invasive intensity/position monitor for hard x-ray beamlines at the European XFEL are discussed. Starting from principle scheme used at LCLS (the XFEL at SLAC, USA) a comparison of possible alternatives and options is made with respect to XFEL planned beam parameters. With help of modeling observable parameters (signal, resolution, range of measurement, etc.) for different setups are obtained. Degradation of the beam due to attenuation and possible damage for the detector itself are also considered. Detector design for a proof-of-principle experiment at a synchrotron X-ray source is proposed.

# Contents

<b>1</b>	<b>Introduction</b>	<b>4</b>
1.1	Requirements for the device at European XFEL . . . . .	5
<b>2</b>	<b>Theory</b>	<b>6</b>
2.1	Overview of X-ray Interactions With Matter . . . . .	6
2.2	X-ray Scattering: . . . . .	7
2.2.1	From one electron: . . . . .	7
2.2.2	From an atom/molecule: . . . . .	8
2.2.3	From a thin film: . . . . .	9
2.2.4	Structure effects: . . . . .	9
<b>3</b>	<b>Simulation</b>	<b>10</b>
3.1	Source Code . . . . .	10
3.2	Adjustment of the code . . . . .	10
3.3	Resolution calculations . . . . .	11
3.4	Materials investigation . . . . .	12
3.4.1	Attenuation . . . . .	12
3.4.2	Crystalline effects . . . . .	12
3.4.3	Heat load estimates . . . . .	12
<b>4</b>	<b>Simulation Results</b>	<b>13</b>
4.1	Beam transmission . . . . .	13
4.2	Crystalline effects . . . . .	14
4.3	Intensity maximization . . . . .	15
4.4	Position measurement . . . . .	15
4.4.1	Beam size effect . . . . .	16
4.4.2	Position resolution . . . . .	17
4.5	Intensity measurement . . . . .	17
4.5.1	Intensity resolution . . . . .	18
4.5.2	Beam position effect . . . . .	18
4.6	Heat load . . . . .	19
<b>5</b>	<b>Setup design</b>	<b>20</b>
<b>6</b>	<b>Conclusions and summary</b>	<b>23</b>

# 1 Introduction

European XFEL (X-ray Free Electron Laser, XFEL.eu) is a powerful X-ray light source for scientific purposes being constructed in Hamburg. Compared to other operating and planned FELs European XFEL has some distinct features: a wide energy range (from 0.28 keV up to 25 keV) and pulse train mode which means that up to 3000 pulses separated by 220 ns can be produced with a repetition rate of 10Hz ([1], [2]). The commissioning is planned to start in 2015; user operation is planned to start the same year.

For accurate tuning of the machine as well as for stable and smooth operation during user experiments information about the photon beam should be gathered. There are two approaches to photon diagnostics: invasive and non-invasive. The former means that most part of the beam is absorbed or severely distorted by the detector, which is acceptable for commissioning mode but is can't be used for on-line diagnostics during user operation.

Intensity and position measurements provide essential information on FEL condition. Average intensity of the beam provides a good figure of merit for SASE process in the undulator system while single pulse intensity measurement can characterize the stability of the machine. Beam position information is necessary for alignment of the beam optics system and is needed for users to keep their samples in the beam. Also temperature drifts and Earth's crust movement can make contributions to beam position [3], so there is a need to calibrate these effects and take them into account during operation.

Several devices can incorporate both functions, namely: position sensitive ion chamber, fluorescence-based beam position monitor [4] and scattering-based beam position monitor if we consider non-invasive ones. For application at hard X-ray FEL beamlines fluorescence detectors suffer too much heat load, especially in the bunch train mode. Ion chambers must be designed very carefully in order to operate reliably without suffering from charge-recombination under high dose conditions while maintaining vacuum compatibility [7]. The most straightforward solution avoiding the issues mentioned above is the scattering beam position monitor with a low Z scatterer to minimize photoabsorption.

Using scattering signals to provide photon diagnostics was suggested before [5] and recently a relatively simple design was proposed for intensity-position measurements [6]. The principal scheme for this device can be seen in Figure 1.

The principle is as follows: part of the beam passing through the foil is scattered in the backward direction. Backscattering geometry is used because inelastic scattering peaks in the backward direction, which gives less information on the scatterer structure and more on the beam itself. If the beam is centered then signals on opposite diodes should be equal, otherwise they differ. By calibrating that difference one can measure the displacement of the beam in two directions (one per pair of diodes situated oppositely). Also by measuring sum of the signals from four diodes one can obtain a certain fraction of the beam's intensity. This can be used for absolute measurement of beam's intensity after proper calibration. Thereby, this device can in principle provide intensity and position information for individual pulses as well as averaged over a time interval. Such

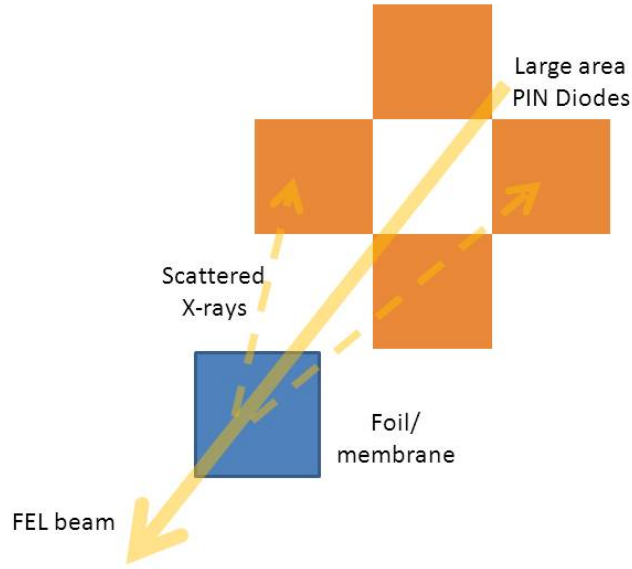


Figure 1: *Principal scheme of a backscatter monitor*

devices are already in use at LCLS and SACLA. Experimental characterization at a synchrotron source (SPring-8) has been done for such a device [7]. Considering European XFEL features mentioned above, a separate investigation of optimal configuration of the intensity-position monitor is required. Different configurations should be considered with respect to the demands of users and beam transportation system at the XFEL.eu.

## 1.1 Requirements for the device at European XFEL

Requirements for the device were obtained from beamline users [8] as well as machine performance group [9]: General:

- > 98% transmission
- No noticeable wavefront distortion (not considered in this work, supposed to be negligible for thin films)
- Vacuum compatible
- Photon energy range  $3 \div 25$  keV
- Pulse energy range  $0.03 \div 2.5$  mJ

For 2D position measurement:

- Resolution  $\sim 1\% \sigma_{FWHM}$  which can go down to  $5\mu m$  for 24.8 keV photon energy, according to [3]
- Working range (x,y) at least 1mm for measuring long term effects [3]

For intensity measurement:

- $\sim 1\%$  relative accuracy
- Measurement should be independent from beam position in the working range

## 2 Theory

### 2.1 Overview of X-ray Interactions With Matter

There are three competing processes in X-ray interactions with matter: photoelectric absorption, scattering (elastic/inelastic) and electron-positron pair production [10]. At XFEL.eu, the energy range supposed for hard X-rays beamlines is  $3 \div 25$  keV. Pair production does not take place because photon's energy should be more than  $2m_e c^2 \approx 1.022$  MeV for it to occur.

Photoelectric absorption cross-section is highly dependent on  $Z$  and energy:  $\sigma_{photoel} \sim \frac{Z^n}{E^{3.5}}$  [10] where  $n$  is between 4 and 5. Edge effects are not considered, because for materials with  $Z < 17$  K-edge is below 3 keV. For example, in the case of beryllium, the cross-section is negligible compared to scattering only for energies close to 25 keV and for energies near 3 keV it's two orders of magnitude more [11].

Photoelectric absorption can lead to Auger electron emission and X-ray fluorescence. The former doesn't affect the acquired signal, so it is not taken into account here. Ratio of fluorescence photons to absorbed ones is given by *fluorescence yield*  $\omega_K$  (photon energy is greater than the K-edge, which means that most electrons will be ejected from K shell). This quantity can be obtained from tables or empirical formulae, such as:  $\omega_K = (1 + \frac{a}{Z^4})^{-1}$  where  $a \approx 10^6$  [13]. For Be  $\omega_K \approx 2.6 \cdot 10^4$  which means that fluorescence is negligible for all the energy range. If we take heavier elements, for example Si, with  $\omega_K = 0.038$  and  $\sigma_{photoel}$  two-three orders of magnitude larger than  $\sigma_{scatter}$ , fluorescence can't be neglected. Nevertheless, we can use the fact that fluorescent emission can be considered angle-independent for our energy range. Thus, its contribution to diode signals will change slowly with beam movement ( $\sim \Delta\Omega \sim \Delta x^2$ ) compared to scattering signal, which may peak in the space between the diodes. This in turn suggests that fluorescence signal can be considered a constant fraction of beam's intensity. Fluorescence contribution was not taken into account in further considerations and simulations.

The main source of information for the device is X-ray scattering, which is explained in more detail in the next section.

## 2.2 X-ray Scattering:

### 2.2.1 From one electron:

The cross-section for X-ray scattering from a free electron is given by Klein-Nishina formula (see [14] for example):

$$\frac{d\sigma_{KN}}{d\Omega} = \frac{r_e^2}{4} \left( \frac{k'}{k} \right)^2 \left[ \frac{k'}{k} + \frac{k}{k'} + 4(\boldsymbol{\varepsilon}' \boldsymbol{\varepsilon})^2 - 2 \right], \quad (2.1)$$

where  $r_e = \frac{e^2}{m_e c^2}$  is the classical electron radius,  $\boldsymbol{\varepsilon}$  and  $\boldsymbol{\varepsilon}'$  are polarization vectors of the incoming and scattered beam respectively,  $k$  is incoming photon's momentum, and  $k'$  is given by:  $k' = \frac{k}{1 + k \frac{\hbar}{m_e c} (1 - \cos \theta)}$  where  $\theta$  is the polar angle. In the limit of  $k' \rightarrow k$  (elastic scattering) one can obtain the classical Thompson formula:

$$\frac{d\sigma_T}{d\Omega} = r_e^2 (\boldsymbol{\varepsilon}' \boldsymbol{\varepsilon})^2.$$

FEL beams usually have a high degree of polarization so we consider the incoming beam having a settled polarization. The diodes, however, are insensitive to polarization, so the overall signal on a diode will be a sum of those over  $\boldsymbol{\varepsilon}'$ .

Let us consider FEL beam propagating along  $z$  axis and polarized along  $x$ . The direction of the scattered beam is given by polar angle  $\theta$  and azimuth  $\varphi$ . There are two possible polarizations for the scattered beam and unit polarization vectors  $\tilde{\mathbf{e}}_1, \tilde{\mathbf{e}}_2$  can be obtained by a spatial rotation from two basis polarization vectors  $\mathbf{e}_1, \mathbf{e}_2$  for the incident beam. First we rotate  $\theta$  with  $\varphi = 0$  (which is just rotation around  $y$  axis). Then we rotate  $\varphi$  which means rotating around  $z$ -axis:

$$\mathbf{e}_1 = \begin{pmatrix} 1 \\ 0 \\ 0 \end{pmatrix}, \mathbf{e}_2 = \begin{pmatrix} 0 \\ 1 \\ 0 \end{pmatrix}, \quad (2.2)$$

The rotation matrix  $S$ :

$$\mathbf{S} = \begin{pmatrix} \cos \varphi & -\sin \varphi & 0 \\ \sin \varphi & \cos \varphi & 0 \\ 0 & 0 & 1 \end{pmatrix} \cdot \begin{pmatrix} \cos \theta & 0 & \sin \theta \\ 0 & 1 & 0 \\ -\sin \theta & 0 & \cos \theta \end{pmatrix}, \quad (2.3)$$

$$\tilde{\mathbf{e}}_1 = \mathbf{S} \mathbf{e}_1,$$

$$\tilde{\mathbf{e}}_2 = \mathbf{S} \mathbf{e}_2,$$

$$\tilde{\mathbf{e}}_1 = \begin{pmatrix} \cos \varphi \cos \theta \\ \sin \varphi \cos \theta \\ -\sin \theta \end{pmatrix}, \tilde{\mathbf{e}}_2 = \begin{pmatrix} -\sin \varphi \\ \cos \varphi \\ 0 \end{pmatrix},$$

Thus we obtain:

$$\sum_{\epsilon'} (\epsilon' \epsilon)^2 = (\mathbf{e}_1 \cdot \tilde{\mathbf{e}}_1)^2 + (\mathbf{e}_1 \cdot \tilde{\mathbf{e}}_2)^2 = \cos^2 \theta \cos^2 \varphi + \sin^2 \varphi = 1 - \sin^2 \theta \cos^2 \varphi, \quad (2.4)$$

leading to the resulting cross-sections:

$$\frac{d\sigma_{KN}}{d\Omega} = \frac{r_e^2}{4} \left( \frac{k'}{k} \right)^2 \left[ \frac{k'}{k} + \frac{k}{k'} + 4(1 - \sin^2 \theta \cos^2 \varphi) - 2 \right], \quad (2.5)$$

Hence, the Thompson formula becomes:

$$\frac{d\sigma_T}{d\Omega} = r_e^2 (1 - \sin^2 \theta \cos^2 \varphi). \quad (2.6)$$

### 2.2.2 From an atom/molecule:

Scattering by an atom has two distinct features: first there are  $Z$  scattering electrons which create a charge distribution according to their wavefunctions. The second point is that elastic and inelastic scattering differ physically instead of one being a limit to the other. In the inelastic case scattering electron is transferred to another energy level, while after elastic scattering it remains on the same. Both this features can be described in terms of atomic form factors  $F(\chi, Z)$  and incoherent scattering functions  $S(\chi, Z)$ , which modify the single-electron cross-section.  $\chi$  here is  $\frac{\sin \theta/2}{\lambda}$ , where  $\lambda$  is the wavelength of the incoming X-rays. The resulting cross sections are given then by [16] :

$$\begin{aligned} \frac{d\sigma_{el}}{d\Omega}(\theta, \varphi) &= \frac{d\sigma_T}{d\Omega}(\theta, \varphi) \cdot |F(\chi, Z)|^2, \\ \frac{d\sigma_{inel}}{d\Omega}(\theta, \varphi) &= \frac{d\sigma_{KN}}{d\Omega}(\theta, \varphi) \cdot S(\chi, Z), \end{aligned}$$

For molecules a similar formalism is used and resulting form factors and incoherent scattering functions are given by [17] :

$$\begin{aligned} |F_{mol}(\chi)|^2 &= \sum_i n_i |F_i(\chi, Z_i)|^2, \\ S_{mol}(\chi) &= \sum_i n_i S_i(\chi, Z_i), \end{aligned}$$

where  $n_i$  is the atomic abundance of  $i$ -th element.

In case the atoms in a molecule are bound ionically, a simple approximation can be made, considering the scattering factors are proportional to the electron density in the atom:

$$|F_{mol}(\chi)|^2 = \sum_i n_i \left| \frac{Z'_i}{Z_i} F_i(\chi, Z_i) \right|^2, \quad (2.7a)$$

$$S_{mol}(\chi) = \sum_i n_i \frac{Z'_i}{Z_i} S_i(\chi, Z_i), \quad (2.7b)$$

where  $Z'_i = Z_i - q$  and  $q$  is the ion charge.



### 2.2.3 From a thin film:

Here we consider a film without any inner structure, e.g. amorphous.

For infinitely thin film with thickness  $dx$ , the intensity scattered in a sufficiently small solid angle  $\Delta\Omega$  is given by:

$$\Delta I = I_{inc} \frac{\rho N_A}{\mu} \left( \frac{d\sigma_{el}}{d\Omega}(\theta, \varphi) + \frac{d\sigma_{inel}}{d\Omega}(\theta, \varphi) \right) \Delta\Omega dx = I_{inc} \frac{\rho N_A}{\mu} \frac{d\sigma_{total}}{d\Omega}(\theta, \varphi) \Delta\Omega dx$$

For a finite thickness  $t$  we should divide the film into infinitely thin layers and consider that a part of the photons leave the beam in each layer thus decreasing the incoming intensity for next layers. The intensity of the beam passing through a uniform media is given by:

$$I(x) = I_0 \cdot \exp^{-\frac{x}{l_a}}, \quad (2.8)$$

where  $I_0$  is the incoming intensity,  $l_a$  is the attenuation length and  $x$  is depth inside the material. Overall intensity scattered in  $\Delta\Omega$  is then:

$$\begin{aligned} \Delta I &= \int_0^t I(x) \frac{\rho N_A}{\mu} \frac{d\sigma_{total}}{d\Omega}(\theta, \varphi) \Delta\Omega dx = \frac{\rho N_A}{\mu} \frac{d\sigma_{total}}{d\Omega}(\theta, \varphi) \Delta\Omega \int_0^t I_0 \cdot \exp^{-\frac{x}{l_a}} dx = \\ &= I_0 \frac{\rho N_A}{\mu} \frac{d\sigma_{total}}{d\Omega}(\theta, \varphi) \Delta\Omega l_a (1 - \exp^{-\frac{t}{l_a}}), \end{aligned}$$

In case of thin film  $t \ll l_a$  and  $(1 - \exp^{-\frac{t}{l_a}}) \approx \frac{t}{l_a}$  thus:

$$\Delta I = I_0 \frac{\rho N_A t}{\mu} \frac{d\sigma_{total}}{d\Omega}(\theta, \varphi) \Delta\Omega. \quad (2.9)$$

### 2.2.4 Structure effects:

Presence of long range order or structure in the film has a certain influence on scattering processes by causing interference effects. Inelastic scattering is insensitive to this, because photon energy is changed and thus coherence is lost. For homogenous amorphous films there is no long range order so no effect is expected. If the film is crystalline than all the intensity from elastic scattering is redistributed so that it is concentrated around certain directions, given by Bragg's Law [15]:

$$2d_{hkl} \cos \phi = \lambda, \quad (2.10)$$

where  $\phi = \frac{\theta}{2}$  is the incidence angle with respect to a crystalline plane defined by Miller indices  $h, k, l$  and  $d_{hkl}$  is the corresponding interplanar distance. For polycrystalline materials that results in Debye-Scherrer rings with intensity of the rings dependent on a single crystallite size. Monocrystalline film will produce isolated high intensity spots dependent on the thickness of the foil and size of the beam (which determines the number of scattering atoms). These effects were not considered qualitatively in my work but a qualitative study can be found in the next chapter.

## 3 Simulation

### 3.1 Source Code

A MATLAB script was developed by Yiping Feng (LCLS) for modeling the monitor [6]. Based on this subsequent scripts were developed for simulating and optimizing device performance. The original code calculates intensity distribution in the plane where the diodes are positioned for a given pulse energy and distance between diode plane and film. Incoming beam is considered point-like and linearly polarized in  $x$  (horizontal) direction. Beam is oriented along the detector axis  $z$ . The beginning of the coordinate system is the point where beam crosses the film plane.

The detector plane is covered with an equally spaced rectangular grid. Then for each element formula (2.9) is implemented.  $\Delta\Omega$  is given by  $\frac{a^2 \cdot \cos(\pi - \theta)}{r^2}$  where  $a^2$  is the area of an element and  $r$  is the distance between the element and the beginning of the coordinate system. Atomic form factor and incoherent scattering function are obtained by interpolating tabulated values given in [16] with a second order polynomial for  $\chi$  range expected at 9 keV photon energy. It should be kept in mind that for other energies this interpolation is no longer valid.

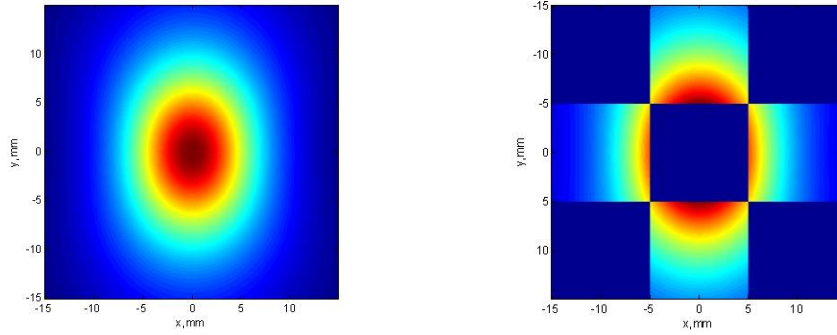


Figure 2: (left)Intensity distribution obtained with code from [18];(right)Intensity distribution restricted to the area covered by diodes

For each diode integration over its area is performed yielding total intensity on each of the diodes.

### 3.2 Adjustment of the code

The code has been modified to account for:

- Beam shift and tilt, by recalculating all the coordinates relevant for scattering with  $z$  axis determined by the beam pointing and the beginning of coordinates determined by the beam position in the film plane;

- Beam of a finite size is simulated by dividing beam intensity into several beams with different positions, covering an area in the film plane, and then summing the scattered intensities;
- $F(\chi)$  and  $S(\chi)$  are interpolated with cubic splines in the  $\chi$  range corresponding to the whole energy range of interest.

### 3.3 Resolution calculations

A script for calculating resolution of position measurements was developed. The measured signal is  $s = \frac{I_1 - I_2}{I_1 + I_2}$ , where  $I_1$  and  $I_2$  are intensities detected on two opposing diodes. There are two independent sources of error we consider for each diode:

- "Poisson" noise which is caused by the fact that scattering is a random process with low probability
- Dark current noise: while we can exclude the mean value of dark current, its variance is random and should be treated as an error

Dark current is usually known in nA, so we need to convert it to a corresponding number of photons per pulse. First we obtain number of e-h pairs created by one photon:

$$N = \frac{E \cdot (1 - \exp^{-\frac{d}{l_a}})}{3.6 \text{ eV}}$$

where 3.6 eV is the energy needed to create an e-h pair and  $d$  is the thickness of diode's active layer.

$$I_{\text{dark}} = \frac{i_{\text{dark}}(A) \cdot t_{\text{int}}}{e \cdot N} \quad (3.1)$$

where  $t_{\text{int}}$  is the integration time of a diode, and  $e$  is the electron charge  $1.6 \cdot 10^{-19}$  Coulomb.

Signal error is:

$$\delta s = \sqrt{\frac{\partial s^2}{\partial I_1} (\delta I_{\text{poi}1}^2 + \delta I_{\text{dark}1}^2) + \frac{\partial s^2}{\partial I_2} (\delta I_{\text{poi}2}^2 + \delta I_{\text{dark}2}^2)} \quad (3.2)$$

Considering shot-to-shot measurements with integration time  $< 220 \text{ ns}$  dark current contribution to the noise can be neglected. In this case  $\delta I_{\text{poi}} = \sqrt{I_{\text{detected}}}$ . Substituting this into 3.2 and evaluating the derivatives yields:

$$\delta s = \frac{2}{(I_1 + I_2)^2} \sqrt{I_2^2 I_1 + I_1^2 I_2}$$

Beam shift  $x$  is obtained from  $s(x)$  curve. It means that  $\Delta s$  leads to an error in  $x$  measuring:

$$\delta x = \frac{dx}{ds} \cdot \delta s = \frac{\delta s}{\frac{ds}{dx}} \quad (3.3)$$

The same approach in case of intensity measurements (measured signal is  $\tilde{I} = I_1 + I_2 + I_3 + I_4$ ) yields:

$$\delta I = \frac{\sqrt{\tilde{I}}}{\frac{d\tilde{I}}{dx}}. \quad (3.4)$$

### 3.4 Materials investigation

#### 3.4.1 Attenuation

Beam passing through the foil will lose a certain part of its intensity due to the absorption and scattering. Intensity of the outgoing beam is then given by (2.8) where  $x$  is set to the film thickness. It is dependent on photon energy and material used through the attenuation length  $l_a$ . The values for  $l_a$  in my work were taken from LBL [12] database.

#### 3.4.2 Crystalline effects

Qualitative analysis is made on basis of conclusions from [7]. For polycrystalline films with grain size  $\sim 1\mu m$  a degradation of resolution was observed because of the highly anisotropic intensity distribution in Debye-Scherrer rings. Even for nanocrystalline films problems may occur if one of the rings crosses the edge of a diode. Signal response to the beam shift becomes nonlinear making calibration difficult and ultimately limiting the resolution too. For European XFEL application one should also consider that rings change their position with photon energy. Scripts were written to determine if at least one ring crosses diode's edge at a given distance  $Z$  for all the expected energy range. Radius of the ring corresponding to reflection plane with Miller indices  $h,k,l$  in the diode's plane is given by:  $r_{hkl} = Z \cdot \tan(2\phi_{hkl})$ , where  $\phi_{hkl}$  is determined by Bragg's Law (2.10).

#### 3.4.3 Heat load estimates

We consider the film damaged if its temperature is higher than  $T_{melt}$  at any given point. First important characteristic is the temperature raise per pulse. We assume that no thermal conductivity occurs during a pulse, so all heat is absorbed in the beam region.

$$\Delta T_{pulse} = \frac{E(1 - e^{-\frac{t}{l_a}}) \cdot \frac{t}{l_a}}{c_p \cdot m_{region}} \approx \frac{E \cdot \frac{t}{l_a}}{c_p \cdot \rho \pi r^2 t} = \frac{E}{c_p \cdot \rho \pi r^2 l_a} \quad (3.5)$$

Considering European XFEL conditions, more significant case is the pulse train regime. One figure of merit can be given by  $\Delta T_{train} = N \Delta T_{pulse}$  where  $N$  is the number of pulses in a train. This is a valid estimate only if thermal conductivity can be neglected, thus we should have a figure of merit for thermal conductivity. Let's consider equilibrium state when all absorbed heat is transferred from the heated region by thermal conductivity. The equilibrium condition is as follows:

$$W = I \cdot (1 - e^{-\frac{t}{l_a}}) \approx I \cdot \frac{t}{l_a} = q \cdot S = \kappa \frac{\Delta T_{cond}}{h} \cdot 2\pi r \cdot t \quad (3.6)$$

where  $W$  is absorbed power,  $I$  is the incoming intensity,  $l_a$  is the attenuation length (dependent on energy),  $t$  is the foil thickness ( $t \ll l_a$ ),  $\kappa$  is the thermal conductivity coefficient,  $r$  is the beam radius, and  $h$  is the transfer length which can be considered equal to  $r$ . Then it follows that:

$$\Delta T_{cond} = \frac{I}{l_a \cdot 2\pi\kappa}$$

$\Delta T_{cond}$  is the maximum temperature rise where all heat is distributed through the whole sample at this temperature. That means if  $\Delta T_{train} > \Delta T_{cond}$  we should use the latter value to estimate if the film is damaged after a pulse train.

If the thermal conductivity is not sufficient to prevent the material from reaching  $T_{melt}$  one can estimate a maximum number of pulses that the film can survive:  $N_{max} = \frac{T_{melt}T_0}{\Delta T_{pulse}}$  where  $T_0$  is the temperature at which the film is kept. We consider  $T_0$  to be 0 Celsius (273 K).

## 4 Simulation Results

Concerning requirements for the device and commercial availability four scatterer options have been chosen for further investigation:

- Be, 100  $\mu m$  thick
- Amorphous  $Si_3N_4$ , 0.5  $\mu m$  thick
- Polycrystalline CVD diamond, 30  $\mu m$  thick
- $B_4C$ , 50  $\mu m$  thick

with the latter not found available with the demanded thickness. Detailed simulations were performed for  $Si_3N_4$  with photon energy 12keV and pulse energy 1.25mJ. Information of the ionic state of the material has been taken from [20] to calculate the form factor according to (2.7). The beam was considered to be point-like which was justified by the simulation in 4.4.1.

### 4.1 Beam transmission

In Fig.3 demanded thicknesses for 98% transmission are plotted in blue and actual thicknesses in green. One can see that none of the considered materials transmit enough intensity at photon energies below 5 keV. This places a lower limit on the energy range the device can be used in effectively. The thickness of the materials can be reduced to allow more transmission at the cost of reducing scattered intensity and hence resolution.

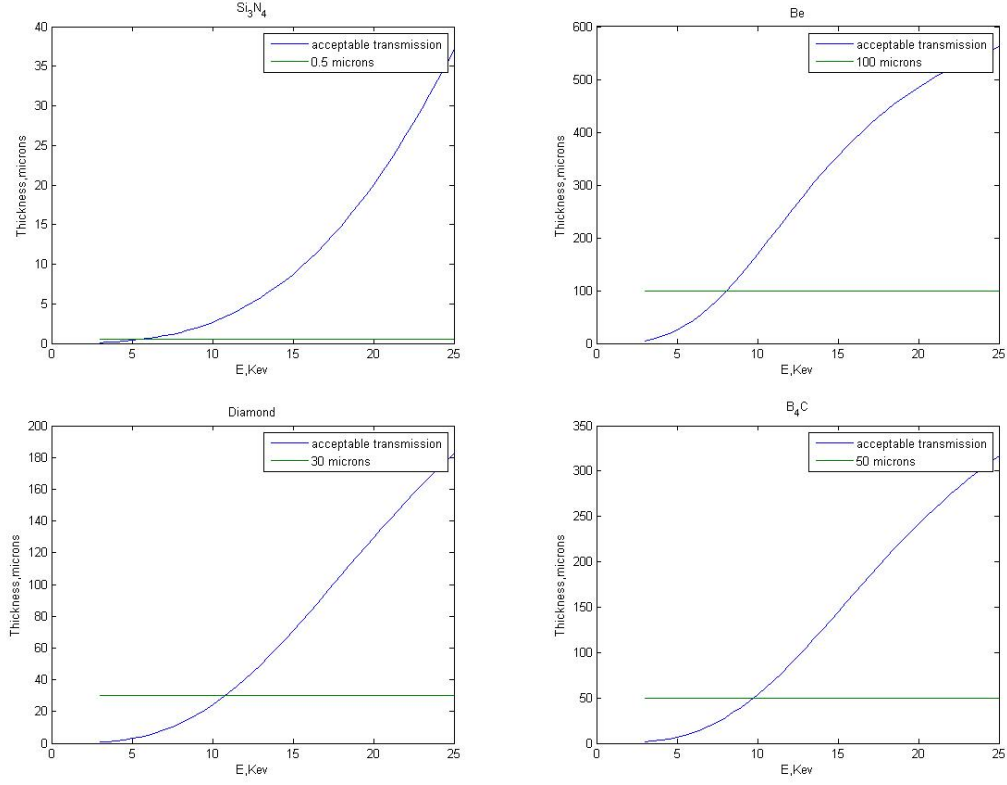


Figure 3: Thickness needed for 98% transmission(blue) and real thickness(green)

## 4.2 Crystalline effects

In Fig.4 are plotted the values of energies when diffraction effects don't cause degradation of the performance are denoted by value 1. One can see that for high energies, at least one Debye-Scherrer ring is always expected to cross the diode's edge.

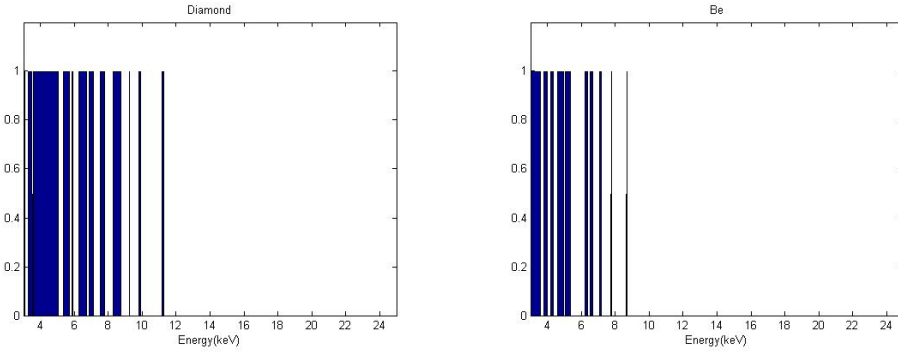


Figure 4: Diffraction effects for diamond and Be: 1-no diffraction rings cross diode's edges, 0-at least one ring crosses diode's edges

### 4.3 Intensity maximization

Fig.5 shows intensity acquired by diodes at various distance between foil and diodes  $Z$ .

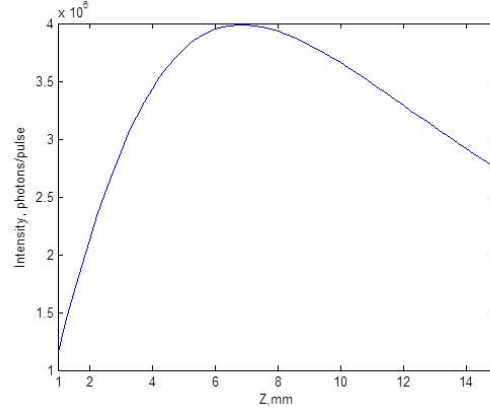


Figure 5:  $I(Z)$

A maximum can be observed at  $Z = 6.75mm$ . In Fig.6 one can see that the position of this peak changes for less than 1mm with photon energy.

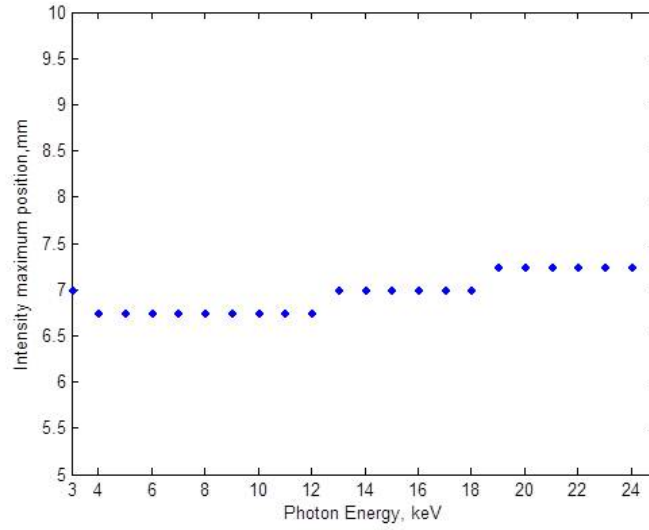


Figure 6:  $Z_{max}(E)$

### 4.4 Position measurement

The signal curves for differing  $Z$  can be seen in Fig.7. One can see that there is a trade-off between linear response range and the slope of the linear part, which determines the

resolution.

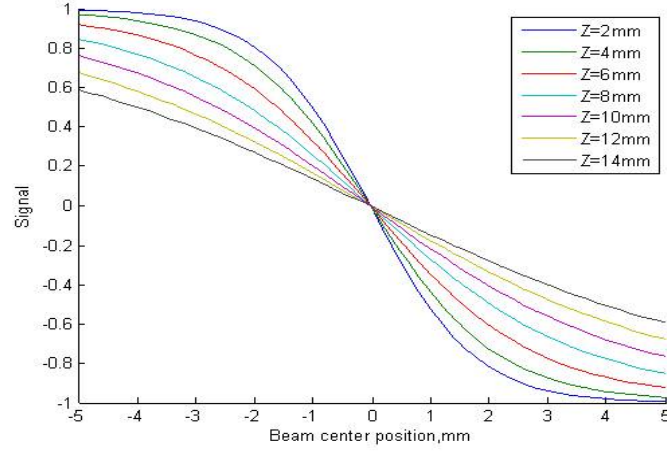


Figure 7: Signal  $s = \frac{I_R - I_L}{I_R + I_L}$  vs. beam position  $x$  for different  $Z$

#### 4.4.1 Beam size effect

Beam is considered to have square form, where beam size is the length of its side. One can see that differences are very small for changing size, and maximum deviation in the  $[-1;1]$  x range was measured to be 3.5%.

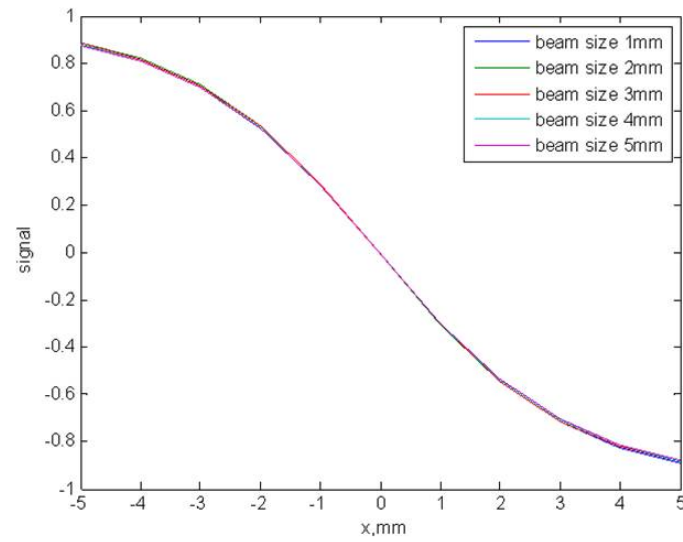


Figure 8: Signal  $s = \frac{I_R - I_L}{I_R + I_L}$  vs. beam position  $x$  for different beam sizes



#### 4.4.2 Position resolution

Position resolution obtained from (3.3), shown in Fig.9, shows a minimum close to the position of intensity maximum in Fig. 5 but  $Z$  is slightly less. For 24.8 keV resolution is worse than the required 1% of beam  $\sigma_{FWHM} \sim 1\mu m$ . In this situation one should consider expected beam position jitters. If we take LCLS, for example, the beam jitters there are on the order of 10% [19] and a close number might be expected at the European XFEL [9]. Considering this value 25  $\mu m$  resolution is still sufficient for position measurements.

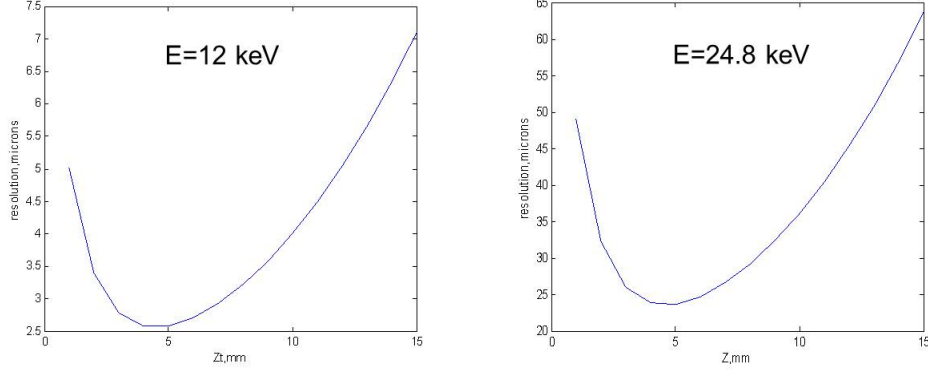


Figure 9: *Resolution vs.  $Z$  for photon energies 12 and 24.8 keV*

#### 4.5 Intensity measurement

In Fig.10 one can see simulated response curve for intensity measurement for  $Z$  equal to 7mm, and photon energy to 12keV.

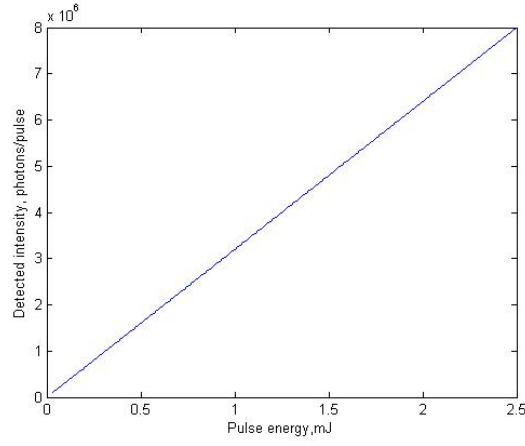


Figure 10: *Signal  $\tilde{I} = I_R + I_L + I_U + I_D$  vs. pulse energy*

#### 4.5.1 Intensity resolution

For same conditions resolution simulation is shown in Fig.12. One can see that even for lowest pulse energy (0.03 mJ here) relative accuracy is better than 1%.

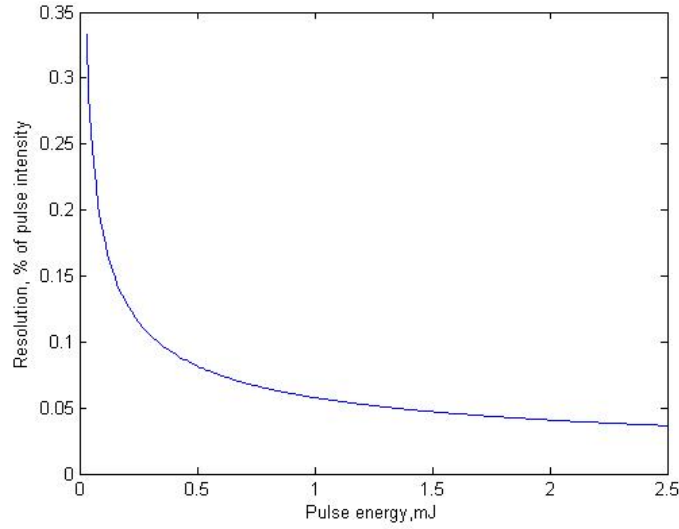


Figure 11: *Relative accuracy (%) vs. pulse energy*

#### 4.5.2 Beam position effect

For pulse energy 1.5 mJ variations in overall intensity resulting from the beam shift were simulated. If one considers shift range 1 mm then maximum relative difference between signals in that range is 0.8%.

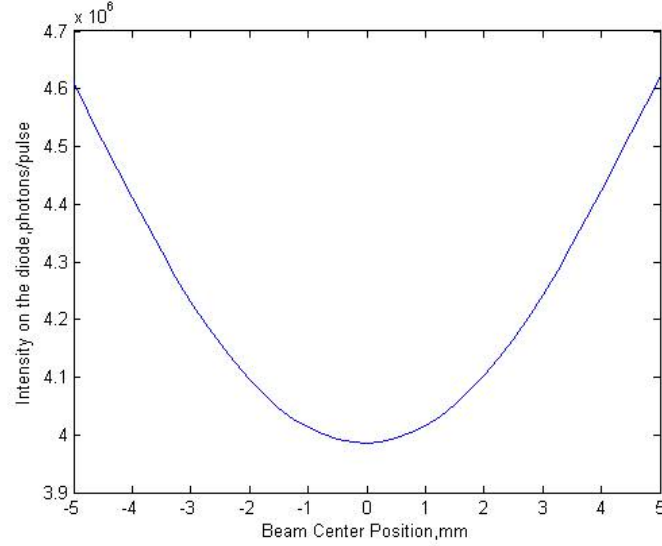


Figure 12: *Signal  $\tilde{I} = I_R + I_L + I_U + I_D$  vs. beam shift for  $Z=7\text{mm}$  and photon energy= $12\text{keV}$*

## 4.6 Heat load

Calculated parameters discussed in 3.4.3 in are given in Fig.4.6. Beam parameters are taken from [3] for beam after the optics system but before a monochromator. It appears

		Average Heat Load	Pulse Train Mode								
		X-ray energy 7.75 keV	X-ray energy 7.75 keV			X-ray energy 12.4 keV			X-ray energy 20.7 keV		
		Pulse energy 2.57 mJ	Pulse energy 2.57 mJ			Pulse energy 1.26mJ			0.708mJ		
	T melt,C	$\Delta T_{\text{cond}},\text{C}$	$\Delta T_{\text{train}}$	$\Delta T_{\text{cond}}$	Nmax whole train	$\Delta T_{\text{train}}$	$\Delta T_{\text{cond}}$	Nmax whole train	$\Delta T_{\text{tr}}$	$\Delta T_{\text{cond}}$	Nmax
Diamond	3550	7,8	5243	1319	17	616	155	137			
Silicon Nitride	1414	1109,3	228905	187800	whole train	27951	22931	whole train	3496	2868	1092
Be	1415	11,4	546	1937	whole train	83	295	whole train			
Boron Carbide	2445	217,9	2486	36889	2655	314	4661	whole train			

that all of the discussed materials withstand the pulse train condition well, except for  $\text{Si}_3\text{N}_4$ . At high energies though, because of lower photoelectric absorption  $\text{Si}_3\text{N}_4$  can withstand nearly half a pulse train.

## 5 Setup design

For characterizing the backscatter monitor experimentally an investigation at a synchrotron light source has been proposed. At a synchrotron source conditions are different from the ones expected at the European XFEL, namely:

- Fluence is very low: in terms of energy it is close to one XFEL pulse per second
- Experiment will be carried out in air which means photon energy  $> 7\text{keV}$ , otherwise the attenuation is too high

Applied to the device this means that the resolution will degrade because of the low intensity. Longer integration times will be required for this reason leading to noticeable dark current noise effects. Heat load investigation is not possible for this experiment. Yet it provides a good proof-of-principle and optimization of scatterer material and  $Z$  (distance) can be carried out experimentally. For this purpose a setup was designed. A projection of the whole setup can be seen in Fig. 13(all dimensions in mm). Diode holder plate and scatterer holder plate are connected to separate bulk bases with countersink screws. One of the bases has a controllable moving stage to optimize distance between foil and diodes.

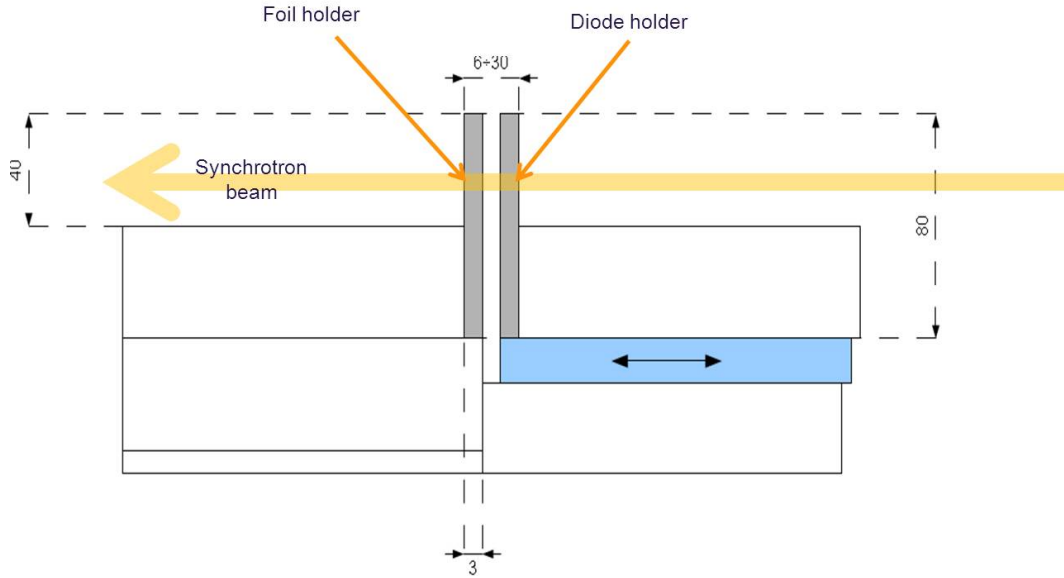


Figure 13: A side projection of designed setup

Diode holder is presented in more detail in Fig.14. Four diodes are put in dimples and fixed with clamps tightened by adjacent screws.

Film holder design is found in Fig. 15. A metal strip (Fig. 16) with films is slid in, as indicated by the arrow and fixed with dimples on its lower side as well as two additional screws depicted as blue circles. Window size in film holding strip is set for

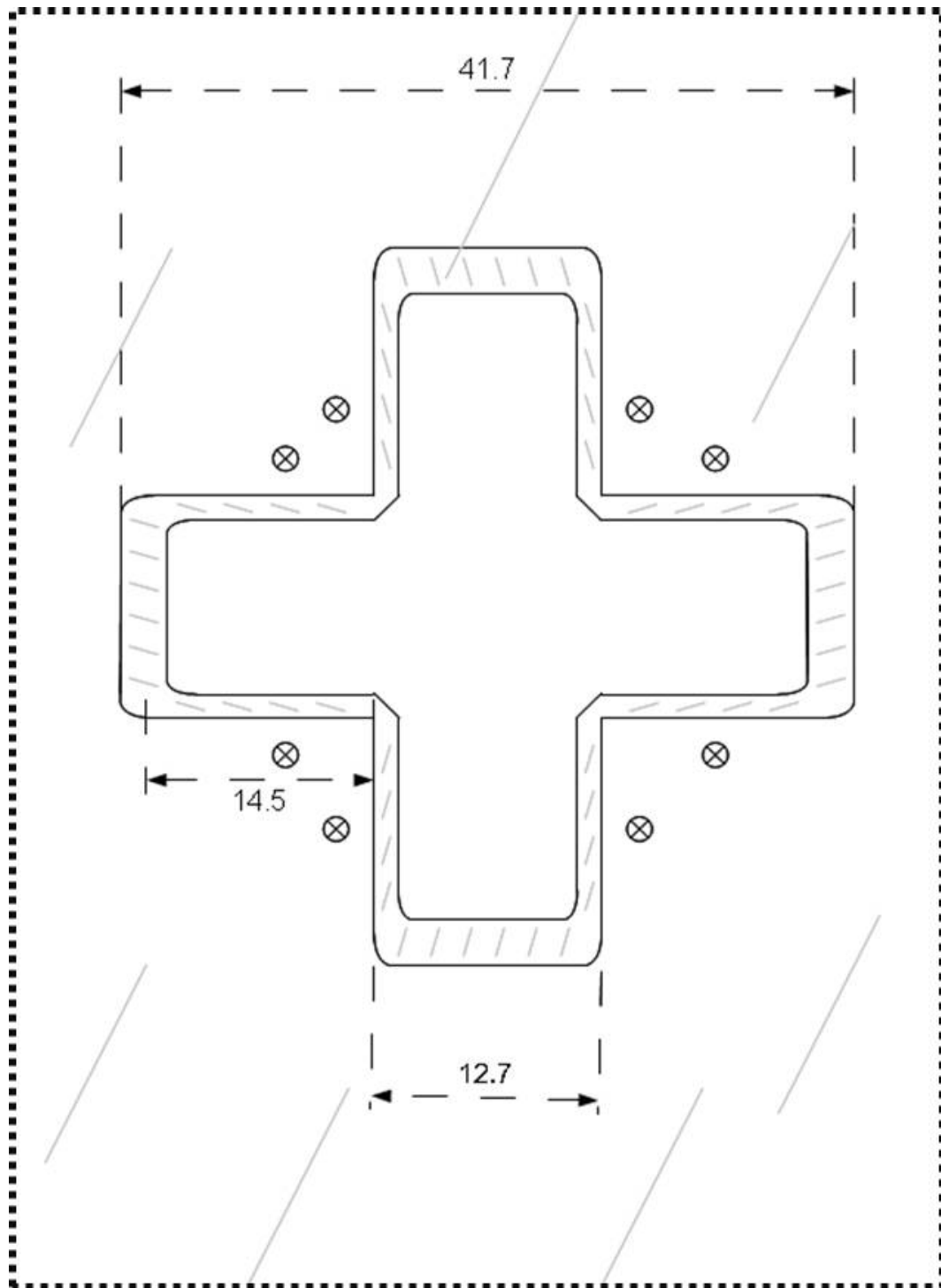


Figure 14: A part of the diode holder plate

each film depending on its size. Then the corresponding specimen is put onto the strip and fixed with clamps that are attached to the strip with screws. This provides an easy

and fast way to change scattering material.

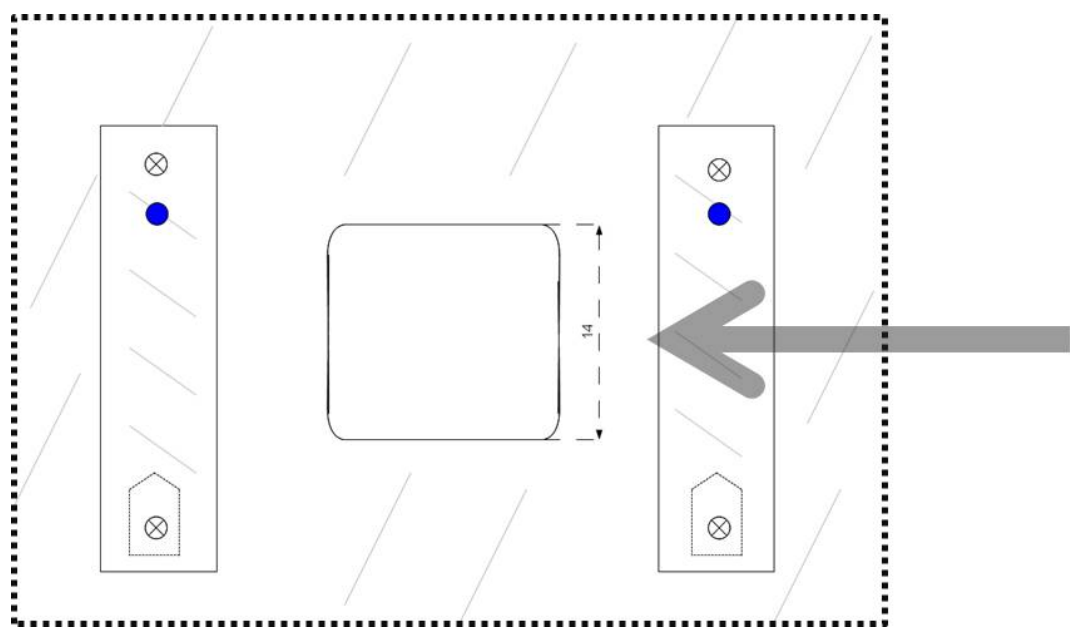


Figure 15: A part of the film holder plate

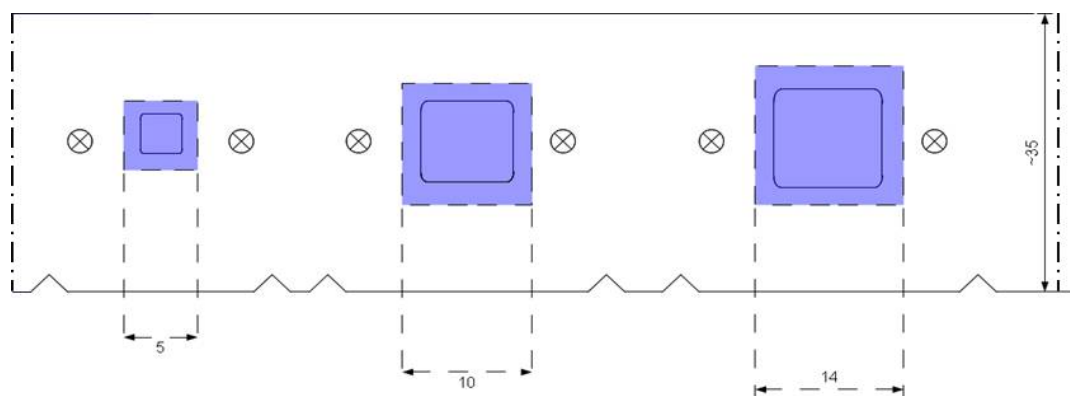


Figure 16: Film holding metal strip

## 6 Conclusions and summary

Possibilities for using backscatter monitor at the European XFEL have been investigated by means of simulation. Four different scattering materials were considered. Performed simulations for the backscatter monitor have shown that:

- The proposed monitor can achieve demanded resolution in position and intensity measurements and beam position range
- An optimal distance between diodes and scatterer should be used, and a value (5mm) has been obtained from simulations
- For energies lower than 5 keV none of the investigated films provide 98% transmission and thickness reduction comes only at a cost of reduced intensity and position resolution
- For low energies and high peak power diamond or Be should work fine, although transmittance is less than demanded (97% at 7.75 keV for diamond)
- For low pulse energies  $Si_3N_4$  is preferred but can't be used in pulse train mode except for high energies ( $>20$  keV)

A design for device characterization at a synchrotron light source has been proposed.

## References

- [1] M. Altarelli et al., *The European X-ray Free-Electron Laser Technical design report* , 2007, DESY 2006-097
- [2] Th. Tschentscher, *Layout of the X-ray Systems at the European XFEL*, 2011, XFEL.EU TN-2011-001
- [3] H. Sinn et al., *X-ray Optics and Beam Transport* , 2011, XFEL.EU TN-11-002
- [4] R. W. Alkire, G. Rosenbaum and G. Evans, *Design of a vacuum-compatible high-precision monochromatic beam-position monitor for use with synchrotron radiation from 5 to 25 keV* , 2000, J. Synchrotron Rad., 7, 61
- [5] A. J. Wootton and D. D. Ryutov, *Compton scattering and photoluminescence for X-ray imaging* , 2003 Review of Scientific Instruments, 73, 1180
- [6] Y. Feng, *LUSI Diagnostics & Common Optics* , February 27-28 2009, SLAC/DESY/SPring-8 3-Way Collaboration
- [7] K. Tono et. al., *Single-shot beam-position monitor for X-ray free electron laser* , 2011, Review of Scientific Instruments, 82, 1180
- [8] A. Mancuso, personal communication
- [9] M. Yurkov & E. Schneidmiller, personal communication
- [10] G. F. Knoll, *Radiation Detection and Measurement*, 3<sup>rd</sup> edition , 2000, Wiley
- [11] XCOM: Photon Cross Sections Database, <http://www.nist.gov/pml/data/xcom/index.cfm>
- [12] Lawrence Berkley National Laboratory Database, <http://henke.lbl.gov/optical.constants/atten2.html>
- [13] R. W. Fink, R. C. Jopson, Hans Mark, C. D. Swift, *Atomic Fluorescence Yields*, 1966, Reviews of Modern Physics, 38, 513
- [14] J. D. Bjorken and S. D. Drell, *Relativistic quantum mechanics*, 1964, McGraw-Hill
- [15] C. Kittel, *Introduction to Solid State Physics*, 2004, 8th ed.
- [16] J. H. Hubbel et al., *Atomic form factors, incoherent scattering functions and photon scattering cross sections*, 1975, J. Phys. Chem. Ref. Data, 4, 471
- [17] D. E. Peplow and K. Verghese, *Measured molecular coherent scattering form factors of animal tissues, plastics and human breast tissue*, 1998, Phys. Med. Biol., 43, 2431
- [18] Y. Feng, personal communication



- [19] J.L. Turner et al., *FEL Beam stability in the LCLS*, Proceedings of 2011 Particle Accelerator Conference, New York, NY, USA
- [20] R. Grun, *The Crystal Structure of  $\beta - Si_3N_4$  ; Structural and Stability Considerations Between  $\alpha$  - and  $\beta - Si_3N_4$* , 1979, Acta Cryst. B35, 800